Uncovering Biological Factors That Regulate Hepatocellular Carcinoma Growth Using Patient-Derived Xenograft Assays

Min Zhu,[1] Lin Li,[1] Tianshi Lu,[1,2] Hyesun Yoo,[3,4] Ji Zhu,[3,4] Purva Gopal,[5] Sam C. Wang,[6] Matthew R. Porembka,[6] Nicole E. Rich (iD) ,[7] Sofia Kagan,[7] Mobolaji Odewole,[7] Veronica Renteria,[7] Akbar K. Waljee,[4,8,9] Tao Wang,[2] Amit G. Singal,[7] Adam C. Yopp,[6] and Hao Zhu (iD) [1]

BACKGROUND AND AIMS: Several major factors limit our understanding of hepatocellular carcinoma (HCC). First, human HCCs are infrequently biopsied for diagnosis and thus are not often biologically interrogated. Second, HCC initiation and progression are strongly influenced by the cirrhotic microenvironment, and the exact contributions of intrinsic and extrinsic tumor factors are unclear. A powerful approach to examine the personalized biology of liver cancers and the influence of host tissues is with patient-derived xenograft (PDX) models. In Asia, HCCs from patients with hepatitis B virus have been efficiently converted into PDXs, but few parallel efforts from the west have been reported.

APPROACH AND RESULTS: In a large-scale analysis, we implanted 93 HCCs and 8 cholangiocarcinomas (CCAs) to systematically analyze host factors and to define an optimized platform for PDX development from both surgical and biopsy samples. *NOD Scid IL-2Rγ$^{-/-}$* (NSG) mice that had undergone partial hepatectomy (PHx) represented the best combination of engraftability, growth, and passageability, but overall rates were low and indicative of a unique intrinsic biology for HCCs in the United States. PDX models preserved the histology and genetic features of parental tumors,

and ultimately, eight models were usable for preclinical studies. Intriguingly, HCC PDXs were differentially sensitive to regorafenib and sorafenib, and CCA PDXs were also highly sensitive to regorafenib.

CONCLUSIONS: PDX models functionalize early and advanced stage HCCs and revealed unique biological features of liver cancers from the United States. (HEPATOLOGY 2020;72:1085-1101).

Hepatocellular carcinoma (HCC) is the sixth most common cancer and second leading cause of cancer-related death worldwide.[1] In the United States, its incidence has doubled over the past two decades due to the growing number of patients with advanced hepatitis C virus (HCV) infections and/or nonalcoholic steatohepatitis (NASH).[2,3] Patients with cirrhosis are at high risk for HCC with a 3%-8% annual incidence rate.[4] Once HCC is diagnosed, the Barcelona Clinic Liver Cancer (BCLC) staging classification divides patients into five stages:

Highlights
- We present a U.S. liver cancer PDX biobank from surgical and biopsy cases.
- Human HCC engraftment in mice increased with greater immunodeficiency and liver injury.
- The frequency and rate of engraftment is low, indicative of unique biological features of HCCs.
- These patient avatars show that there are differential sensitivities to sorafenib and regorafenib reflecting heterogeneous responses seen in the clinic.

0, A, B, C, and D. Stages 0 and A (very early and early) are curable by surgical resection, liver transplantation, or local ablative therapies.[4] However, a minority of patients with HCC are diagnosed with early-stage tumors; most patients with HCC present with intermediate or advanced-stage disease, when only palliative therapies are available. Although patients diagnosed with early-stage tumors can achieve 5-year survival rates exceeding 70% with curative therapies, patients with non-early-stage HCC continue to have median survival rates of 1-2 years despite the introduction of novel therapies.

Historically, the diagnosis of HCC is often made radiographically, without the need for histologic confirmation. As a result, most of the characterized HCC tissue is from surgical specimens obtained from early-stage HCC. This lack of available tissue from patients with intermediate-stage or advanced-stage HCC has led to a dearth of biological knowledge about non-early-stage HCC and likely contributes to slow improvements in palliative therapies over time. It is unknown whether intermediate and advanced HCC represent simple progression from early cases or whether these HCC populations consist of distinct biological entities with unique growth mechanisms, genetic dependencies, and differential sensitivity to systemic therapies.

One way to study the growth dynamics and treatment responses of living tumors is with patient-derived xenograft (PDX) models. For HCC, there are only a few published experiences with PDX models, most of which are derived from Asian patients with noncirrhotic HBV who underwent curative resection.[5-8] Although many Asian patients infected with HBV develop HCC in the absence of cirrhosis, over 90% of U.S. and European patients with HCV, alcohol, and NASH develop HCC in the presence of cirrhosis.[9] Thus, prior PDX models may not be entirely representative of HCCs from the Western world.

In this study, we have established methodologies for PDX development for a large number of U.S. patients with cirrhosis and HCC. Engraftment and passageability rates for HCCs are low, but optimized recipient protocols can increase efficiency. We also found that HCC biopsies can generate PDX models. These HCC PDXs help to characterize the biology of HCC in the Western world and represent an important resource for future studies. This knowledge will help elucidate mechanisms of response to available and experimental therapeutics.

ARTICLE INFORMATION:

From the [1]Children's Research Institute, Departments of Pediatrics and Internal Medicine, Center for Regenerative Science and Medicine, University of Texas Southwestern Medical Center, Dallas, TX; [2]Quantitative Biomedical Research Center, Department of Population and Data Sciences, University of Texas Southwestern Medical Center, Dallas, TX; [3]Department of Statistics, University of Michigan, Ann Arbor, MI; [4]Michigan Integrated Center for Health Analytics and Medical Prediction, Ann Arbor, MI; [5]Department of Pathology, University of Texas Southwestern Medical Center, Dallas, TX; [6]Department of Surgery, University of Texas Southwestern Medical Center, Dallas, TX; [7]Department of Internal Medicine, University of Texas Southwestern Medical Center, Dallas, TX; [8]VA Center for Clinical Management Research, VA Ann Arbor Health Care System, Ann Arbor, MI; [9]Department of Internal Medicine, Division of Gastroenterology and Hepatology, Michigan Medicine and Michigan Integrated Center for Health Analytics and Medical Prediction, Ann Arbor, MI.

ADDRESS CORRESPONDENCE AND REPRINT REQUESTS TO:

Hao Zhu, M.D.
Children's Research Institute
Departments of Pediatrics and Internal Medicine
Center for Regenerative Science and Medicine

University of Texas Southwestern Medical Center
Dallas, TX 75390
E-mail: Hao.Zhu@utsouthwestern.edu
Tel.: +214-648-2850

Methods

MICE

All mice were handled in accordance with the guidelines of the Institutional Animal Care and Use Committee at the University of Texas Southwestern (UTSW) Medical Center. NSG mice were from the UTSW breeding core, and *FRG* mice were from Yecuris Corporation (strain 10-0001). All experiments were done in 6-10-week-old male and female mice. All experiments were done in an age-controlled and sex-controlled fashion unless otherwise noted.

HUMAN SAMPLES

HCC and CCA tumor samples were obtained from patients who underwent surgical resection or percutaneous biopsies. All patients provided informed consent under internal review board #STU 062013-063 for liver tissues and #STU 092013-010 for blood samples. Pathologic diagnosis was confirmed by a board-certified pathologist specializing in gastrointestinal oncology (P.G.) in a blinded fashion. A total of 101 tumor samples were implanted. Patients had an average age of 62 years old (77 males, 24 females).

IMPLANTATION OF TUMORS INTO RECIPIENT MICE

For SQ experiments, multiple tumor fragments of 2-5 mm^3 were implanted with or without PHx. For liver implantation, an incision was made in the abdomen, and a fragment (1-2 mm^3) was implanted and sealed with a small piece of Surgicel to stop bleeding. For *FRG* mice, NTBC water was removed after the surgery and cycled every 7 to 10 days to induce liver injury. Mice implanted with parental tumors were euthanized before any tumor grew to 2 cm in diameter. Tumor growth in liver was examined at the time of euthanasia. To expand a PDX model, tumors were implanted to multiple NSG mice without PHx, snap frozen for future data analysis, fixed with 4% paraformaldehyde for histology, and stocked in 10% DMSO + 90% FBS for future use. Some xenografts were thawed from frozen stocks and re-implanted into NSG mice subcutaneously. After thawing and implanting, mice were maintained the same way as primary xenograft implantation.

HISTOLOGY

Tissue samples were fixed in 4% paraformaldehyde and paraffin embedded. Primary antibodies used were Hep Par1 (OCH1E5) (264M-94; Sigma-Aldrich, St. Louis, MO), EpCAM (#14452; Cell Signaling, Danvers, MA), CK19 (ab15463; Abcam, Cambridge, United Kingdom), CD31 (ab28364; Abcam), CD45 (ab10558; Abcam), and Ki-67 (ab15580; Abcam). Detection was performed with the Elite ABC Kit and DAB Substrate (Vector Laboratories, Burlingame, CA), followed by hematoxylin counterstaining (Vector Laboratories).

RNA EXTRACTION AND QUANTITATIVE REAL-TIME PCR

Total RNA was extracted from tumors and corresponding xenografts using the Invitrogen PureLink RNA mini kit (Carlsbad, CA). Complementary DNA was synthesized using iScript reverse-transcription reagents (Bio-Rad Laboratories, Hercules, CA). Human or mouse gene expression was detected using human or mouse-specific primers. A common glyceraldehyde 3-phosphate dehydrogenase (GAPDH) primer set, which reacts with both human and mouse GAPDH, was used as reference gene. Expression level was normalized to human or mouse sample controls.

DRUG STUDIES WITH PDX MODELS

Tumor fragments (125 mm^3) were implanted in both flanks of 10 NSG mice, with 5 mice for each group. Treatment was initiated when the tumor volume reached approximately 50 to 200 mm^3. Sorafenib and Regorafenib were purchased from LC Laboratories (Woburn, MA). Sorafenib was dissolved with Cremophor EL : ethanol (1:1) for stock and diluted 4-fold with water just before use.[10] Sorafenib (10 mg/kg) was given by oral gavage once a day, and control mice were given diluted vehicle. Regorafenib was dissolved in DMSO at 100 mg/mL for stock solution and then diluted using 1:1 mixture of PEG 300 and 30% captisol.[11] Mice were gavaged once daily with regorafenib (20 mg/kg) or vehicle. Long (*L*) and short diameters (*S*) were measured for each tumor twice a week. Tumor volume was calculated by $V = 1/2*L*S^2$.
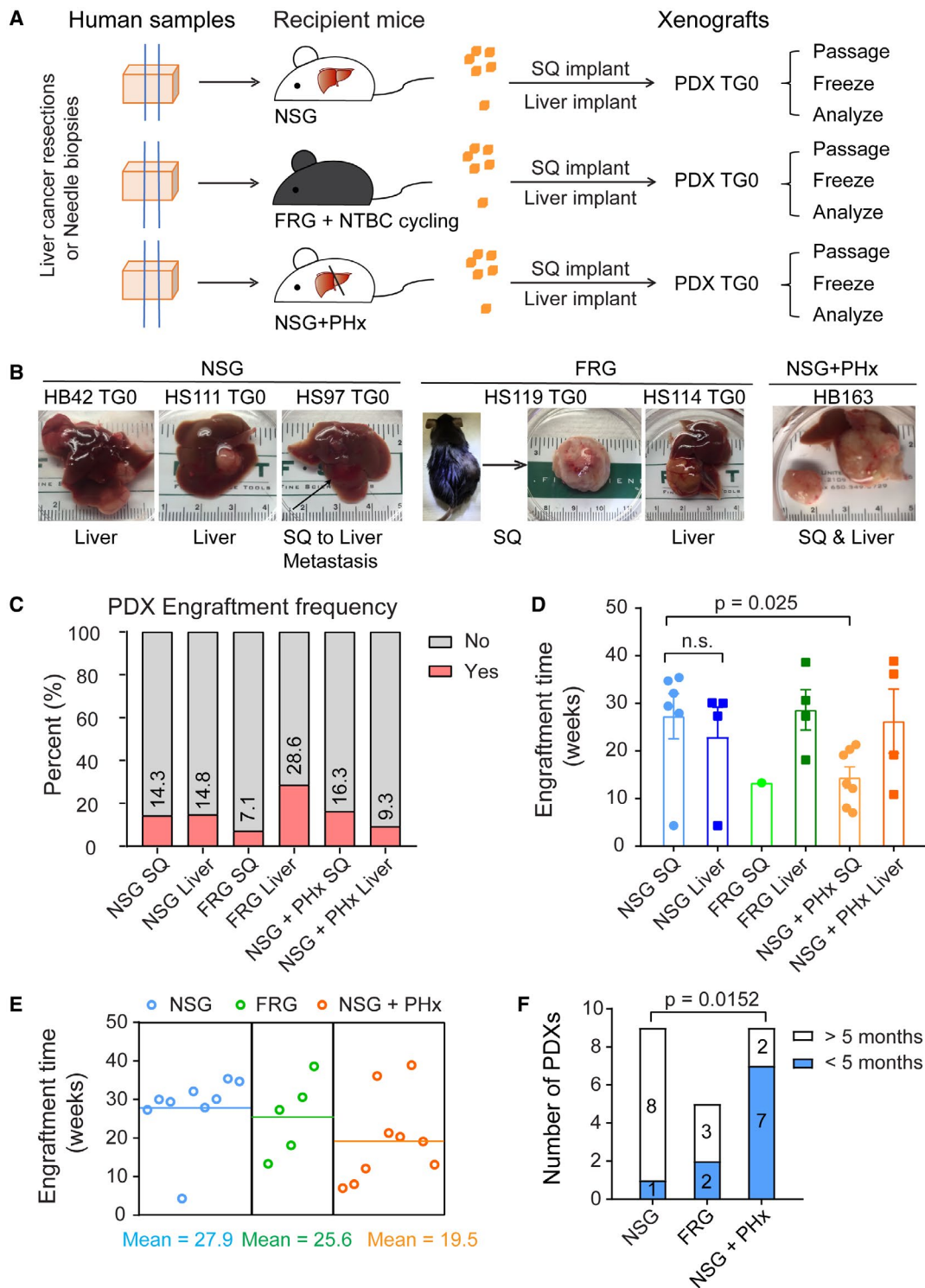
FIG. 1. PDX engraftment in immunodeficient recipients with and without liver injuries. (A) Schema of procedure. (B) Representative pictures of tumors engrafted. (C) Engraftment frequency in the SQ space or the liver in different types of immunodeficient murine recipients. (D) Engraftment time of PDXs in different recipients. Fisher's exact tests were used to compare engraftment times. (E) Overall engraftment time of PDXs in all types of recipients. (F) The number of PDX models that engrafted within 5 months in NSG mice plus hepatectomy versus nonresected NSG mice. Fisher's exact test was used for statistical analysis.

TABLE 1. Engraftment of Liver-Cancer PDX Models in Different Locations and Recipients

| Recipients | Route | Implanted | HCC/CCA PDXs | | Engraftment Time | Passageable Lines | |
			Amount	Percentage	Weeks	Amount	Percentage
NSG	SQ	42	6	14.3%	27.3		
	Liver	27	4	14.8%	22.9		
	Overall	44	9	20.5%	27.9	1	2.3%
FRG	SQ	14	1	7.1%	13.3		
	Liver	14	4	28.6%	28.7		
	Overall	14	5	35.7%	25.6	1	7.1%
NSG + PHx	SQ	43	7	16.3%	14.4*		
	Liver	43	3	9.3%	26.3		
	Overall	43	9	20.9%	19.5	7	16.3%
Total		101	23	22.8%	24	9	8.9%

*P = 0.025 when compared with the NSG-SQ group.

## WHOLE-EXOME SEQUENCING, PROCESSING, AND MUTATION CALLING

Genome DNA was extracted from parental tumors and corresponding xenografts using the Qiagen all-prep DNA/RNA mini kit (Hilden, Germany). DNA was submitted to Admera Health (South Plainfield, NJ) for whole-exome sequencing. We used the QBRC pipeline (github.com/Somatic-pipeline/QBRC-Somatic-Pipeline) for somatic mutation calling. Exome-seq reads were aligned to the GRCh38 genome by BWA-MEM.[12] Picard was used to add read-group information, and sambamba was used to mark PCR duplicates. The calculation of read coverage is performed after duplicate removal. A genome analysis toolkit (GATK)[13-15] was used to perform base-quality score recalibration and local realignment around Indels. MuTect,[16] VarScan,[17] Shimmer,[18] SpeedSeq,[19] Manta,[20] and Strelka2[21] were used to call single-nucleotide polymorphisms (SNPs) and indels. A mutation called by 3 or more of any of these algorithms was retained. ANNOVAR was used to annotate SNPs and indels.[22] All SNPs and indels were combined and kept only if there were at least seven total (wild-type and variant) reads in the blood normal sample and at least three variant reads in the parental tumor or xenograft sample. Only mutations found in COSMIC (https://cancer.sanger.ac.uk/cosmic) were kept. The visualization of mutations by oncoplot is generated by the function *oncoplot* in R package *maftools*.

RNA-Seq AND DATA ANALYSIS

Total RNA was extracted from tumors using the Invitrogen PureLink RNA mini kit. Libraries were prepared with the Ovation RNA-Seq Systems 1-16 (NuGEN Technologies, San Carlos, CA), and indexed libraries were multiplexed in a single-flow cell and underwent 75 base pair single-end sequencing on an Illumina NextSeq500 (San Diego, CA) using the High Output kit v2 (75 cycles) at the UTSW Children's Research Institute Sequencing Facility. To compare RNA expression between parental tumor samples that engrafted versus did not engraft, RNA was extracted and submitted to Admera Health for paired-end RNA-seq. The sequence reads were aligned to the GRCm38 with STAR.[23,24] Read counts were generated for the annotated genes by featureCounts.[25,26] Differential gene analysis was performed use edgeR, with a false discovery rate of less than 0.05 as the cutoff.[27,28] Heatmaps to visualize the data were generated using the R *heat.map2* package. GSEA analysis was performed with a preranked gene list by log fold change.[29] PCA analysis was performed using the R *prcomp* function.

STATISTICAL ANALYSIS

The data in most figures reflect multiple experiments performed on different days using mice from different litters. Two-tailed Student t tests (two-sample equal variance) were used to test the
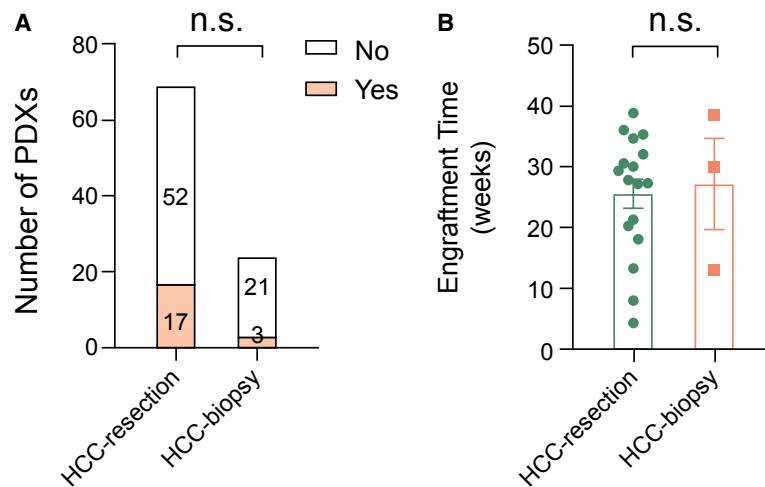
FIG. 2. Comparison of PDX engraftment in surgical versus biopsy samples. (A) Engraftment frequency of PDXs in surgical versus biopsy samples of patients with HCC. (B) Engraftment frequency of PDXs in surgical versus biopsy samples of patients with HCC (n = 17, n = 3). Fisher's exact test was used for (A). Abbreviation: n.s., not significant.

significance of differences between two groups. Fisher's exact tests and Mann-Whitney U tests were used where specifically indicated. In all figures, statistical significance is represented as mean ± SEM (*$P < 0.05$, **$P < 0.01$, ***$P < 0.001$, †$P < 0.05$, and ‡$P < 0.01$).

Results

HCCs ENGRAFT AT LOW RATES IN IMMUNODEFICIENT MICE WITHOUT LIVER DAMAGE

First, we implanted fresh surgical liver tumor specimens in the subcutaneous (SQ) space of *NOD Scid IL-2Rγ$^{-/-}$* (NSG) mice (Fig. 1A). NSG mice were selected because they are the most immunodeficient mice available. We quantified tumor engraftment defined as growth (at any anatomical location) to greater than 5 mm in diameter within 12 months (Fig. 1B). For SQ implantation, the engraftment rate was 14.3% (6 of 42 cases; see Table 1 and Fig. 1C), and the engraftment time was 27.3 weeks (Fig. 1D). Interestingly, in four of these six cases, engraftment was in the form of metastasis to the liver without detectable growth of tumors in the SQ space (Fig. 1B and Supporting Table S1).

Given the long times and low engraftment rates, we aimed to determine what factors influence engraftment, growth rates, and passageability of liver-cancer PDX models. The SQ approach is convenient to assess for engraftment because one can visualize and palpate for tumor growth, but it is possible that the skin microenvironment was suboptimal for liver-cancer engraftment. Because there are likely local pro-growth signals emanating from normal to malignant liver tissues, we also implanted tumors in normal, undamaged NSG livers using an orthograft approach. When tumors were implanted in the liver, the engraftment rate was 14.8% (4 of 27 cases), although this was more challenging to assess because laparotomy was not used to detect early-stage PDX tumors before terminal liver harvesting. The average engraftment time in liver was 22.9 weeks, but this time reduction (compared to 27.3 weeks for SQ) was not statistically significant (Fig. 1D). Another caveat is that it was more difficult to implant larger or multiple tumor fragments within the liver due to tissue fragility and bleeding risk. Thus, orthografting into the liver is inherently less efficient.

The overall engraftment rate for either SQ or liver implantation was 20.5% (9 of 44 cases), and the average engraftment time was 27.9 weeks (Table 1 and Fig. 1E). Surprisingly, the growth of tumors often
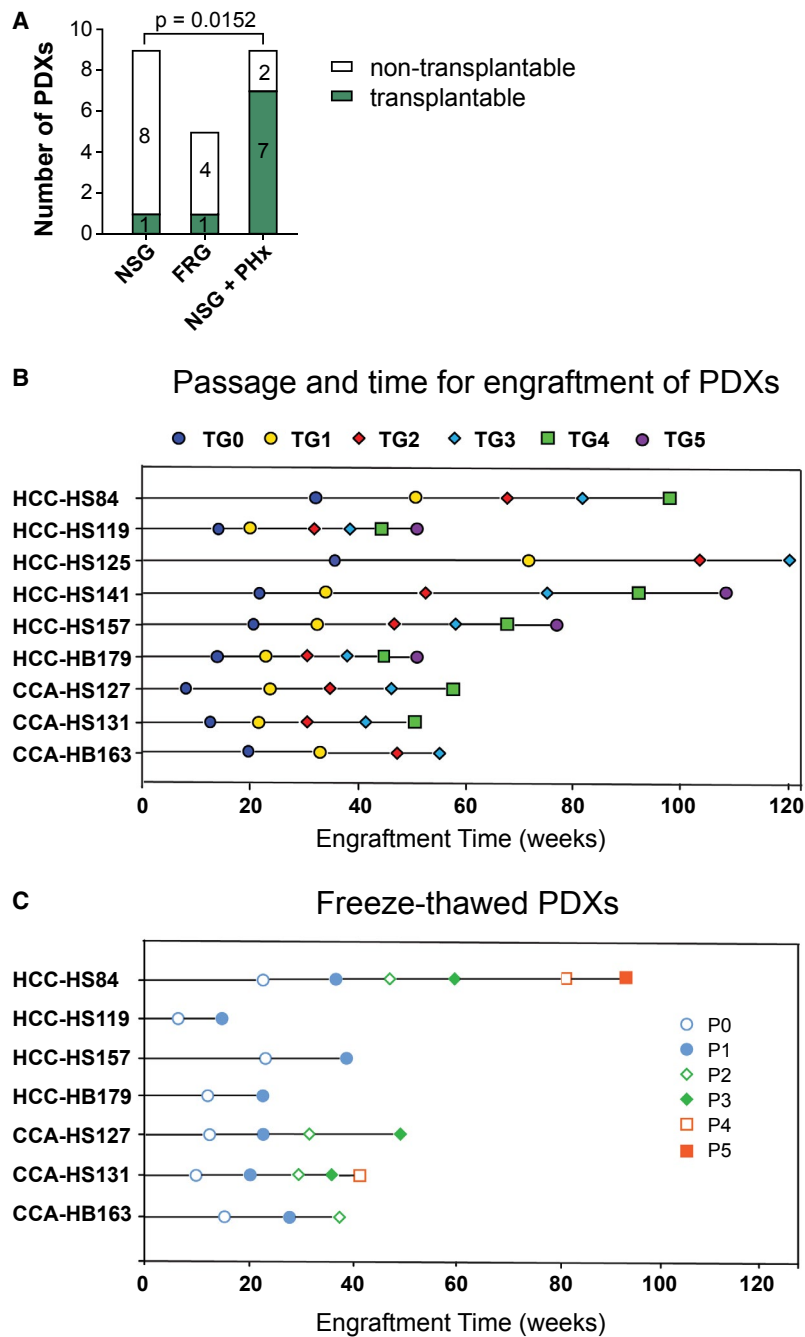
FIG. 3. The serial passageability of liver-cancer PDX models. (A) This shows the passageability of PDXs generated in three types of recipients. Fisher's exact test was used for statistical analysis. (B) Time required for each PDX model to engraft and passage. Once engrafted, tumors were passaged into additional NSG mice to expand the PDX lines. HCC-HS84 was generated from NSG mice. HCC-HS119 was generated from FRG mice. All other lines were generated from NSG mice that had undergone PHx. (C) Engraftment time for frozen and thawed PDX tumors. CCA-HS127, CCA-HS131, HCC-HS84, HCC-HS119, HCC-HS157, CCA-HB163 and HCC-HB179 can be expanded.

took more than 5 months (27 weeks), making these challenging tumor models to develop (Fig. 1E,F). This likely reflected the slow-growth biology of human HCCs and is consistent with the doubling time of HCCs, which has been reported to be 6-12 months.[30]
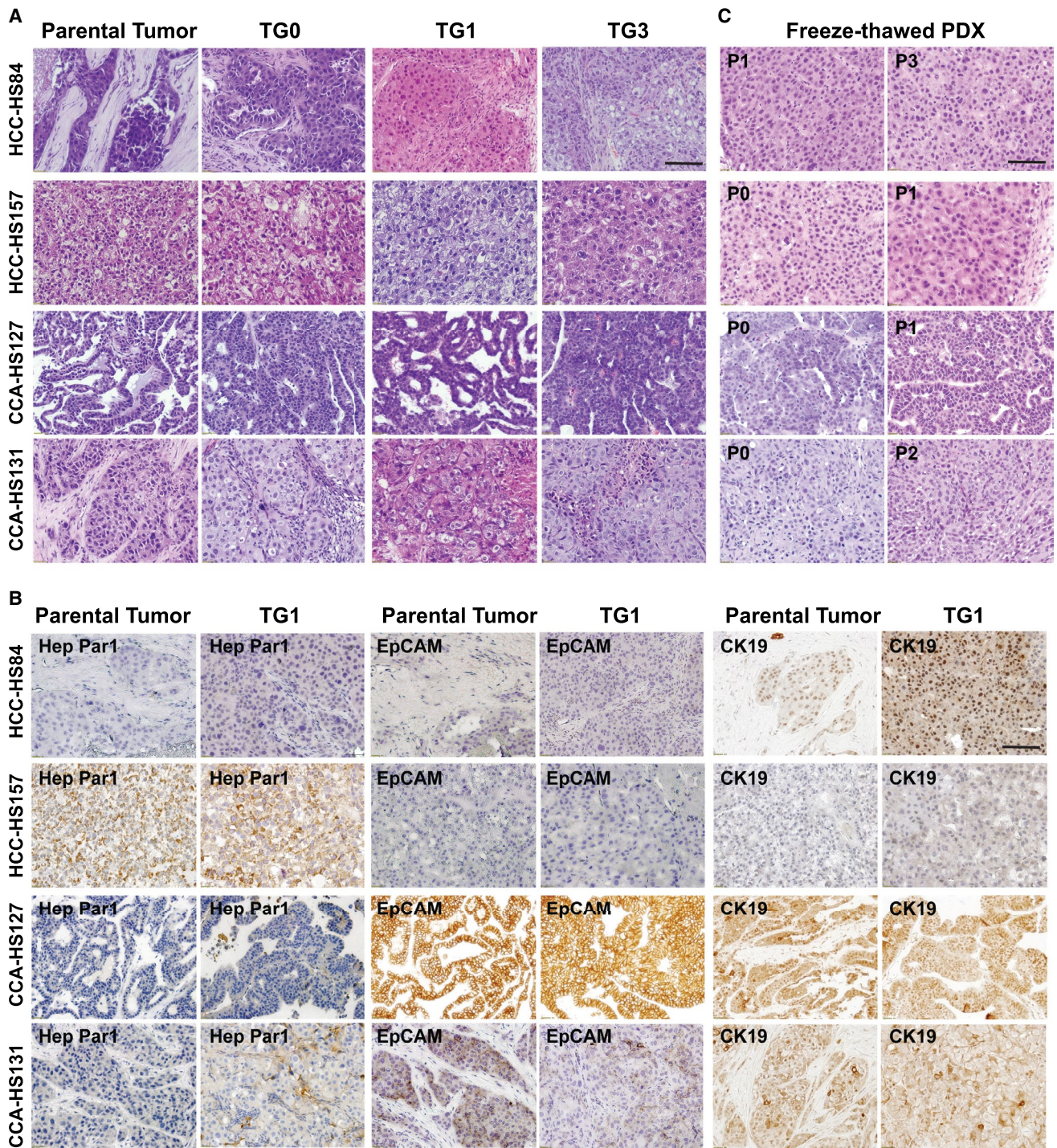
FIG. 4. PDXs maintain the features of parental tumor histology. (A) H&E staining of parental tumors and passaged PDX lines. Scale bar = 100 μm. (B) Immunohistochemistry staining of parental tumor samples and PDXs with anti-Hep Par1, anti-EpCAM, and anti-CK19 antibodies. Scale bar = 100 μm. (C) H&E staining showed that thawed PDXs have a similar histology as the primary PDX and patient tumor. Scale bar = 100 μm. Abbreviation: TG, tumor graft.

PDX ENGRAFTMENT IS ENHANCED WITH GENETIC AND SURGICALLY INDUCED LIVER INJURIES

Because liver cancer often arises in the context of diseased liver tissues, we hypothesized that the host environment would be a critical variable. A tumor microenvironment that integrates liver injury, inflammation, and regeneration might accelerate PDX growth. We attempted to transplant tumors into a mouse model with chronic liver damage caused by hereditary tyrosinemia.[31] Due to a defect in an enzyme involved in tyrosine metabolism, the livers of *Fumarylacetoacetate hydrolase* (*Fah*)$^{-/-}$; *Rag1*$^{-/-}$; *IL-2Rγ*$^{-/-}$ (*FRG*) mice accumulate a toxic metabolite called fumarylacetoacetate and die from liver failure within 2-4 months. To effectively treat this liver disease, mice and human patients are normally given nitisilone or NTBC (2-[2-nitro-4-trifluoromethyl-benzoyl]-1,3-cyclohexanedione), a drug that clears fumarylacetoacetate and maintains a healthy liver.[31] If kept alive for over 6 months on intermittent treatment, *Fah* knockout mice can develop cirrhosis and HCC,[32] indicating that these mice can support the growth of endogenous liver cancers.

Fourteen human liver tumors were transplanted into *FRG* mice, then NTBC was withdrawn and cycled (see Methods) to induce liver damage in the host livers. Tumors were simultaneously implanted in the liver and SQ space of the individual *FRG* mice. Among the 14 cases, five engrafted (four in the liver and one in the SQ space; see Table 1). This increased the engraftment rate in liver from 14.8% to 28.6%, suggesting that the damaged liver microenvironment could promote HCC engraftment in the liver (Fig. 1C). Improvements in overall engraftment frequency between FRG and NSG (35.7% vs. 20.5%) was not accompanied by a significantly shortened engraftment time (25.6 vs. 27.0 weeks) (Table 1 and Fig. 1E). The specific engraftment frequency of SQ tumors was lower in the FRG versus NSG mice (7.1% vs. 14.3%) (Fig. 1C), suggesting that pro-cancer microenvironmental factors were acting locally and not through the systemic circulation.

Importantly, we learned that an orthograft approach in *FRG* could increase PDX-engraftment frequency but did not shorten engraftment time. We reasoned that the deeper immunodeficiency of NSG as compared with *FRG* could have provided an important benefit. Because it would be difficult to make *FRG* more immunodeficient, we asked whether introducing liver damage to NSG would allow us to synergize the deeper immunodeficiency of NSG with the liver injury associated with *FRG*. We stimulated regeneration in NSG mice by performing a 40% partial hepatectomy (PHx) of the left lateral lobe at the time of liver tumor implantation. This is a less aggressive surgery than the standard 60%-70% PHx, but can be more easily performed and allows for a higher survival rate. For 43 patient cases, we implanted liver tumors into both SQ and liver locations in each mouse subjected to PHx. Seven of 43 tumors engrafted in the SQ space (16.3%) and 4 of 43 cases engrafted in the liver (9.3%). Two of these cases overlapped, thus resulting in a total of 9 of 43 cases that engrafted (20.9%) (Table 1 and Fig. 1C). Although the engraftment frequency did not increase substantially for either SQ or liver implantations, the engraftment time for SQ cases significantly decreased to 14.4 weeks compared with 27.3 weeks for NSG implantations without hepatectomy (*P* value = 0.025; Fig. 1D). Seven of the 9 PDX lines generated in NSG mice with hepatectomy engrafted in less than 5 months, whereas only one of nine generated in the NSG mice without surgical resection engrafted in less than 5 months (Fig. 1F). As mentioned previously, *FRG* did not shorten the time to engraftment. Overall, SQ implantation into NSG mice with PHx provided the most advantages in terms of speed and (as will be discussed subsequently) serial passageability of PDX models.

PDX MODELS CAN ALSO BE GENERATED FROM LIVER CANCER BIOPSIES

Some patients do not undergo surgery due to metastatic disease or poor functional status but many have undergone biopsy as part of their diagnostic workup. Patients with advanced HCCs could benefit from PDX models that reveal therapeutic sensitivities. Because biopsies are derived from advanced BCLC–stage HCCs, we hypothesized that these could harbor more aggressive cancer cells that would increase engraftment and PDX growth. To address this, we analyzed the cases in which we implanted biopsy-derived tissues into the various recipient models described

previously. Seventeen of 69 HCC surgical samples (24.6%) and 3 of 24 HCC biopsy samples (12.5%) resulted in engraftment (Fig. 2A and Supporting Table S2). For biopsies, there was not a significant difference in engraftment frequency in different recipient types, potentially due to low case numbers. The average engraftment time was also similar for surgical and biopsy samples (Fig. 2B). Taken together, the data did not support the hypothesis that biopsy cases from advanced HCCs display a more aggressive biology that can be detected in a PDX assay. As a caveat, the reduced mass of biopsy versus surgically derived tissues could have suppressed engraftment efficiency. We also implanted six surgical and two biopsies from patients with CCA. Two of the surgical and one of the biopsy samples engrafted (Supporting Table S2), hinting at an overall higher engraftment rate for CCA versus HCC, regardless of whether the tissue came from a surgery or biopsy. What is clear is that biopsy samples from patients with liver cancer can engraft into useful PDX models. Overall, 23 of 101 (22.8%) primary liver cancers obtained through surgery or biopsy grew macroscopically in the primary PDX transplant setting within 12 months.
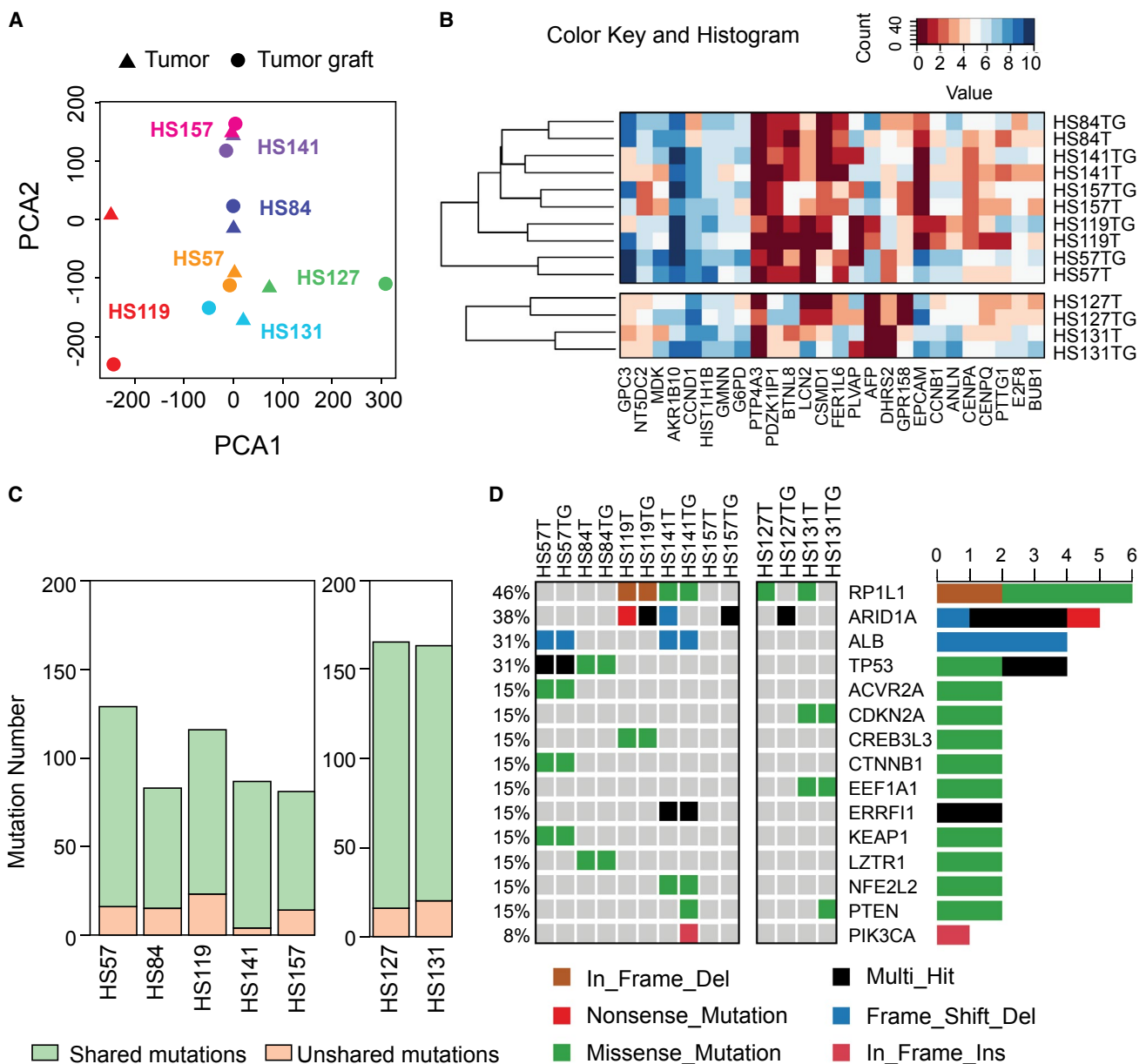
FIG. 5. HCC PDXs retain the genomic expression and mutational profiles of parental tumors. (A) PCA analysis of RNA-seq data from seven pairs of parental tumors and PDX samples. HS57, HS84, HS119, HS141, and HS157 are histological HCCs. HS127 and HS131 are CCAs. (B) Clustering of samples based on evaluation of highly expressed genes in liver cancer. (C) Whole-exome sequencing in parental tumors and PDX models. (D) Oncoplot of mutations in parental tumors and PDXs. We focused on 35 commonly mutated genes in liver cancer based on the The Cancer Genome Atlas analysis. COSMIC mutations or exome mutations compared with 1,000 genomes are shown. Abbreviations: ACVR2A, activin A receptor type 2A; AFP, alpha fetoprotein; ALB, ALBUMIN; AKR1B10, aldo-keto reductase family 1 member B10; ANLN, anillin actin binding protein; ARID1A, AT-rich interaction domain 1A; BTNL8, butyrophilin like 8; BUB1, BUB1 mitotic checkpoint serine/threonine kinase; CCNB1, cyclin B1; CCND1, cyclin D1; CDKN2A, cyclin dependent kinase inhibitor 2A; CENPA, centromere protein A; CENPQ, centromere protein Q; CREB3L3, cAMP responsive element binding protein 3 like 3; CSMD1, CUB and Sushi multiple domains 1; CTNNB1, catenin beta 1; DHRS2, dehydrogenase/reductase 2; E2F8, E2F transcription factor 8; EEF1A1, eukaryotic translation elongation factor 1 alpha 1; ERRFI1, ERBB receptor feedback inhibitor 1; EPCAM, epithelial cell adhesion molecule; FER1L6, fer-1 like family member 6; GMNN, geminin DNA replication inhibitor; G6PD, glucose-6-phosphate dehydrogenase; GPC3, glypican 3; GPR158, G protein-coupled receptor 158; HIST1H1B, H1.5 linker histone, cluster member; KEAP1, kelch like ECH associated protein 1; LCN2, lipocalin 2; LZTR1, leucine zipper like transcription regulator 1; MDK, midkine; NFE2L2, nuclear factor, erythroid 2 like 2; NT5DC2, 5′-nucleotidase domain containing 2; PDZK1IP1, PDZK1 interacting protein 1; PIK3CA, phosphatidylinositol-4,5-bisphosphate 3-kinase catalytic subunit alpha; PLVAP, plasmalemma vesicle associated protein; PTEN, phosphatase and tensin homolog; PTP4A3, protein tyrosine phosphatase 4A3; PTTG1, PTTG1 regulator of sister chromatid separation, securing; RP1L1, RP1 like 1; T, tumor; TG, tumor graft; TP53, tumor protein p53.
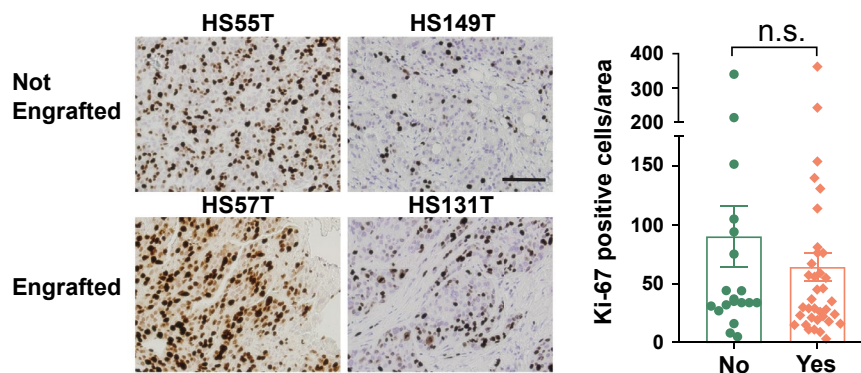

FIG. 6. Comparison of tumors that did and did not engraft in the PDX assays. Representative images of Ki-67 staining of patient tumors that did and did not engraft (left). Scale bar = 100 μm. Statistical analysis of Ki-67-positive cells (right, n = 20, n = 37). Abbreviation: n.s., not significant.

PDXs CAN BE PASSAGED, FROZEN, THAWED, AND EXPANDED

For PDX models to be useful for future studies, they not only had to grow in the primary transplant setting, but they needed to be serially passageable. To determine this, we re-implanted fragments of the liver tumor to additional NSG mice without PHx to determine whether they could be passaged and how many passages could be sustained. Many PDXs, even if they engrafted initially, did not grow after subsequent passaging. In nine PDX lines that engrafted in uninjured NSG mice, only one could be serially transplanted (11.1%). In the five lines that engrafted in *FRG* mice, one could be serially transplanted (20%). However, in the nine lines that engrafted in NSG + PHx mice, seven could be serially transplanted (Fig. 3A) (78%). Thus, host liver resection/regeneration was associated with increased passageability of the PDX lines. The biological mechanisms are unknown, but our data suggested that local or circulating regeneration factors might select for tumor clones that are serially transplantable. Out of the 23 PDXs that engrafted, 15 could be passaged at least once, and nine could be passaged more than 3 to 4 times (Fig. 3B). Six of the 15 stopped growing after two to three passages. For all passages, we collected and snap froze PDX fragments (~125 mm^3) in 10% DMSO/90% fetal bovine serum (FBS) to bank tumor stocks. Seven of the lines could be thawed and re-implanted successfully. These lines include HCC-HS84, HCC-HS119, CCA-HS127, CCA-HS131, HCC-HS157, CCA-HB163, and HCC-HB179 (Fig. 3C). HCC-HS141 could not be successfully thawed but the primary tumor has been passaged for more than 6 times. Altogether, we have
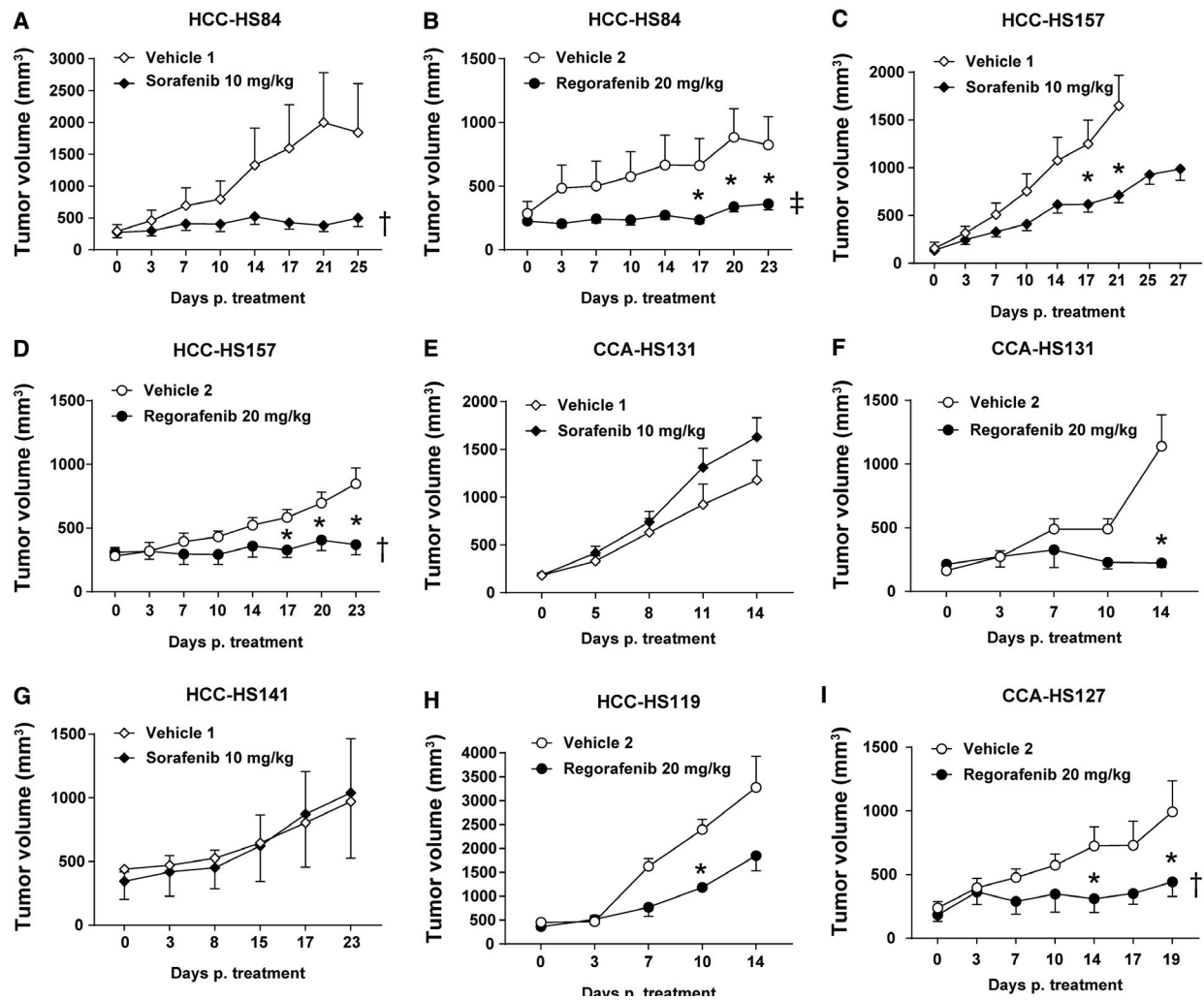
FIG. 7. Differential sensitivity of HCC and CCA-PDX lines to sorafenib and regorafenib. (A,C,E,G) HCC or CCA PDX lines treated with sorafenib (n = 5 to n = 10). (B,D,F,H,I) HCC or CCA PDX lines treated with regorafenib (n = 5 to n = 10). Two-tailed Student *t* tests were used to determine statistical differences between treatments at the same individual time points (shown by asterisks), and Mann-Whitney U tests were used to identify statistical differences between growth curves (shown by cross).

generated eight PDX lines that can be thawed from frozen stocks or maintained as live tumors in mice. In summary, NSG mice undergoing PHx are the optimal hosts for HCC PDX models because of increased engraftment rate, reduced engraftment time, and increased serial passageability after freeze–thaw cycles.

PDXs MAINTAIN PARENTAL TUMOR FEATURES AT THE HISTOLOGIC AND TRANSCRIPTOMIC LEVELS

Tumor architecture, histology, growth, and invasiveness of PDX models and their corresponding primary tumors were compared. To confirm the human origin of these PDX tumors, we performed quantitative real-time PCR to show that the PDX lines expressed human rather than mouse genes. We found that eight originated from human cells (Supporting Fig. S1). We compared the histology of these eight lines with their parental tumors. Hematoxylin and eosin (H&E) staining for PDXs harvested after different passages showed that PDXs and parental tumors were minimally changed over time (Fig. 4A and Supporting Fig. S2A,C). Clusters of differentiation (CD) 45 staining was used to identify and exclude PDXs that resembled lymphomas (data not shown). Eight pairs of PDXs and parental tumors were stained with
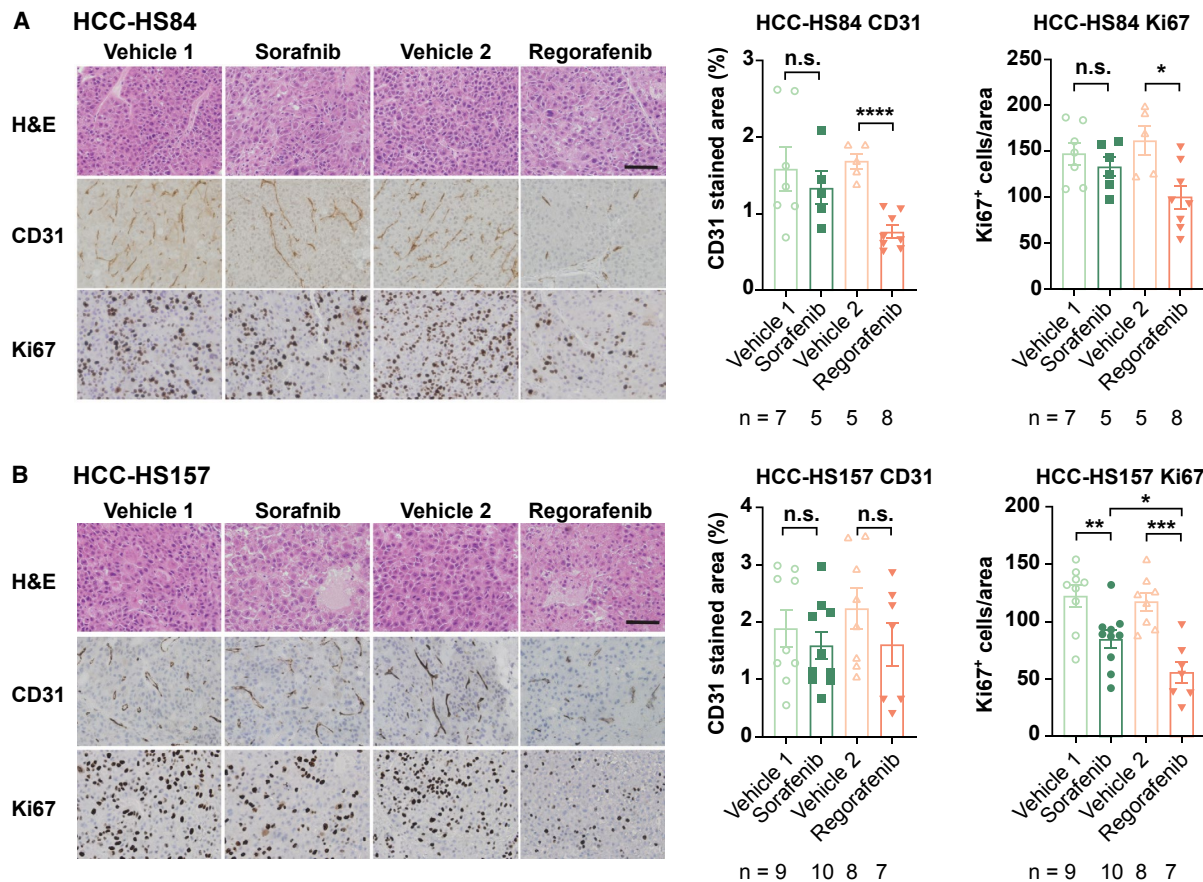
FIG. 8. Effect of regorafenib and sorafenib on angiogenesis and cell proliferation in PDX models. (A) Representative images of H&E, angiogenesis (CD31), and proliferation (Ki-67) of HCC-HS84 PDX treated with sorafenib or regorafenib (left). Statistical analysis of CD31-positive area and Ki-67-positive cells (right). Scale bar = 100 μm. (B) Representative images of H&E, angiogenesis (CD31), and proliferation (Ki-67) of HCC-HS157 PDX treated with sorafenib or regorafenib (left). Statistical analysis of CD31-positive area and Ki-67-positive cells (right). Scale bar = 100 μm. Abbreviation: n.s., not significant.

Hep Par1, EpCAM (epithelial cell adhesion molecule), and CK19 (cytokeratin 19), markers of hepatic and biliary differentiation. HCC PDXs and primary HCCs expressed the same levels of these markers. As expected, CCA cases were Hep Par1–negative and CK19-positive. Representative images are shown in Fig. 4B and Supporting Fig. S2B,D. PDX histology was also maintained after thawing and passaging, making it possible to use the PDX models for future studies (Fig. 4C and Supporting Fig. S2A,C).

Whole-exome and RNA-sequencing (RNA-seq) was used to determine whether mutation and expression signatures were preserved. This kind of analysis, along with histologic evaluation, can help to determine whether key features of the original cancer are retained. Principal component analysis (PCA) analysis was not able to separate the RNA-seq transcriptomes of seven pairs of tumor and PDX from the same patient (Fig. 5A). Clustering based on highly expressed genes in liver cancer resulted in the pairing of PDXs with their corresponding parental tumors (Fig. 5B). Whole-exome sequencing analysis also showed that most mutations were retained in the PDXs when compared with parental tumors (Fig. 5C). HCC driver mutations were also frequently shared by PDXs and patient tumors (Fig. 5D).

CLINICAL OR GENETIC FEATURES COULD NOT PREDICT ENGRAFTMENT OF TUMOR TISSUES

We aimed to determine whether clinical variables such as tumor differentiation correlated with

engraftment. Among 69 surgical HCC cases, 43 cases were moderately differentiated, and nine of these successfully engrafted (21%; see Supporting Table S2). Seventeen were poorly differentiated, and five engrafted (29%). When comparing the engraftment for "moderate," "moderate to poor," and "poor" HCCs, there was a nonsignificant trend of increasing engraftment from 21% to 25% to 29%. However, 3 of 17 poorly differentiated HCCs were serially transplantable, whereas 0 of 43 moderately differentiated HCCs were transplantable (Supporting Table S2; Fisher's exact test; P = 0.02). Surprisingly, the well-differentiated HCC samples could also engraft, although the number of cases was not high enough to evaluate the engraftment rate. Previous reports of Asian HCC PDX models showed that engraftment correlated with tumor cell proliferation as measured by Ki-67. In our cohort, Ki-67 staining on 20 engrafting and 37 nonengrafting primary tumors showed no significant differences in the frequency of Ki-67-positive cells (Fig. 6). To determine whether we could identify transcriptomic predictors of engraftment, we also performed deep RNA-seq on cohorts of parental tumors that either did or did not engraft in PDX assays (n = 17 and n = 19). However, we did not identify gene sets that could reliably distinguish between engrafting and nonengrafting cases using a combination of gene set enrichment analysis (GSEA) and logistic regression analyses with lasso regularization and elastic net regularization. In addition, clinical features such as alanine aminotransferase, aspartate aminotransferase, and other serum markers could not predict engraftment (data not shown).

PDX MODELS SHOW DIFFERENTIAL SENSITIVITY TO SORAFENIB AND REGORAFENIB

We sought to ask whether liver-cancer PDXs could help define therapeutic sensitivities of treatments used in the clinic. Recently, the number of first-line and second-line systemic treatment options for advanced HCC has increased to include four multikinase inhibitors and two PD-1 inhibitors, and it has not been clear how to choose which therapy and in which order. Here, we used our PDX models to serve as patient avatars for the choice between the first-line and second-line HCC multikinase

inhibitors sorafenib and regorafenib. For sorafenib, two of three HCC PDX models (HCC-HS84, HCC-HS141, and HCC-HS157) showed a substantial response and one did not (Fig. 7A,C,G), indicating that these models can help to discern sorafenib sensitivity. A CCA-PDX model showed no response to sorafenib, as would be expected (Fig. 7E). The same PDX models were tested with regorafenib, which is approved for second-line HCC treatment in patients who progress on sorafenib.[33] More of these models showed sensitivity to regorafenib, but one of the four HCC models was only modestly sensitive (Fig. 7B,D,H). This indicates that regorafenib could have a higher response rate in the first-line setting and may be appropriate for treatment-naive as well as sorafenib-resistant patients. The most surprising result was that the CCA-PDX model was exquisitely sensitive to regorafenib, which was previously unknown (Fig. 7F,I).

We also performed histological and molecular analyses of treated versus untreated PDX tumors in an effort to reveal mechanisms by which sorafenib or regorafenib could impede tumorigenesis. We measured the anti-angiogenesis effects by using immunohistochemistry of CD31, which is an endothelial marker that allows us to quantify vessels, and we measured proliferation using Ki-67 (Fig. 8). Both drugs had an effect on proliferation, but regorafenib had a more pronounced effect in both PDX lines. Although sorafenib did not have a significant effect on vascular density as measured by CD31, regorafenib had a significant effect in the HCC-HS84 PDX line. Thus, these drugs have a different magnitude of anti-angiogenesis and antiproliferative effects in different lines, and this can partially explain the sensitivity of each line.

Discussion

PDX models have the potential to uncover new biological information about individual patient-derived liver tumors that have not been adulterated by prolonged growth on plastic under artificial nutrient conditions. Our goal was to understand tumor intrinsic and extrinsic features that would affect tumor biology using PDX engraftment, growth, and passageability as in *in vivo* assays. We first attempted to pinpoint the tumor extrinsic host factors that regulate liver cancer growth. In general, it has been difficult to assess the impact

of the tumor microenvironment on clinically relevant liver tumor models. Within genetically engineered mouse models, it is difficult to isolate tumor intrinsic and extrinsic factors. Also, commonly used HCC cell lines have been so intensely selected for rapid growth that they may not respond to more subtle environmental cues that would otherwise have a greater impact on slower growing tumors. In our experience, it was surprising that the location of implantation (SQ or liver) did not have a major influence on tumor growth. It is possible that the technical challenges associated with liver orthograft implantation disadvantaged that approach when compared with SQ implants, which could accommodate more transplanted tissue.

Not surprisingly, inducing liver injury in immunodeficient mice could promote tumor growth. It is known that tumor initiation is promoted by liver damage, but it is less well understood if the growth of established tumors is enhanced by liver injury. Our data show that even established HCCs can engraft and grow more efficiently when liver injury is introduced through genetic liver damage (*Fah* deletion) or surgical resection (PHx). Interestingly, our experiments support a model in which both signals acting locally in *FRG* mice and in circulation in the context of hepatectomized NSG mice could promote cancer growth. Deeper immunosuppression was also important, as tumors generally grew better in NSG as compared with *FRG* mice. This information about non-cell autonomous regulators of HCC growth allowed us to optimize our efforts to functionalize living tumor tissues. We recommend performing 40% PHx to promote growth and long-term passageability of HCCs implanted into the SQ space of NSG mice.

In regard to comparing host models, there are limitations to our study that need to be highlighted. Because of time constraints that occur after clinical liver resections, we were not able to implant primary patient tumor tissues into the three different host mouse models at the same time. Each host model requires 3-5 mice, which is why performing 10-15 surgeries at the end of the clinical workday was not feasible. Instead, our study retrospectively compared the engraftment efficiencies between different hosts; therefore, we cannot say that for each patient, one engraftment approach is definitively better than another. However, we did implant two established PDX models into all three of the hosts and we found that PHx could modestly improve the growth of one

of the models within the liver as compared with FRG or no PHx (Supporting Fig. S3). Although this indicates that PHx is likely to be an important instigator of engraftment or growth, this is anecdotal data. Another caveat is that we cannot exclude the effects of the surgical procedure itself when we perform PHx in NSG mice. Sham operations without PHx would have provided better controls. Despite these limitations, we believe that there is robust evidence that liver injury exemplified by PHx can promote PDX engraftment in heavily immunosuppressed mice.

There were also tumor-intrinsic features of the HCCs that influenced PDX growth. A study by Gu et al. showed that more than 60 viable HCC-PDX models have been generated from Chinese patients. These PDXs readily engraft, grow, and are used for drug studies.[7] Interestingly, our experience with U.S. patients did not mirror that study, despite implanting over 100 patient cases. In general, engraftment frequency, growth rates, and passageability were very low in comparison to the Asian studies. We are confident that there were no technical issues impairing PDX engraftment, as our group has also generated 30 gastric cancer PDX models from 70 implanted (43% success rate, unpublished), even considering the fact that these PDXs were generated from esophagogastroduodenoscopy-derived biopsies that are generally more scant in mass and cellularity. Our data suggest inherent biological differences among liver cancers from different geographic locations, either due to genetic background or etiology.

Overall, we implanted 93 HCC samples and eight CAA samples in different recipient mice to generate PDX models. Our results showed that immune deficiency and liver injury could improve engraftment and PDX passageability. Using the PDX lines generated with this study, we were able to test the differential sensitivity of sorafenib and regorafenib in both HCC and CCA PDXs. Furthermore, we also found that PDX lines can be generated from surgical samples as well as biopsy samples, making it possible to preclinically test drugs for patients with advanced liver cancer. In the future, machine learning algorithms could also be used to identify potential predictors of engraftment and treatment response. We have not yet been able to do this because of limited statistical power, but larger studies in the future could permit the use of these approaches. Our study reports an important experience in a large number of patients with liver cancer

and lays the foundation for future efforts to functionalize HCCs and CCAs from patients.

Data and Software Availability

The sequencing data reported in this paper has been deposited into the European Genome-phenome Archive (EGA) database. The EGA access ID is EGAS00001004020.

Author Contributions: M.Z. and H.Z. designed the experiments. M.Z. and L.L. performed all mouse experiments. T.L. and T.W. performed all genomic analysis. H.Y., J.Z., and A.K.W. performed statistical analysis of the RNA-seq data for predictors of engraftment. P.G. performed pathological analysis. S.W., M.P., N.E.R., A.G.S., A.Y., and H.Z. obtained the human tumor samples and the clinical data. S.K., M.O., and V.R. assisted with the experiments and obtained the human samples. M.Z., A.G.S., and H.Z. wrote the manuscript.

REFERENCES

1) Tang A, Hallouch O, Chernyak V, Kamaya A, Sirlin CB. Epidemiology of hepatocellular carcinoma: target population for surveillance and diagnosis. Abdom Radiol (NY) 2018;43:13-25.

2) El-Serag HB. Hepatocellular carcinoma: recent trends in the United States. Gastroenterology 2004;127:S27-S34.

3) White DL, Kanwal F, El-Serag HB. Association between nonalcoholic fatty liver disease and risk for hepatocellular cancer, based on systematic review. Clin Gastroenterol Hepatol 2012;10:1342-1359.e2.

4) Bruix J, Sherman M, American Association for the Study of Liver Diseases. Management of hepatocellular carcinoma: an update. HEPATOLOGY 2011;53:1020-1022.

5) Huynh H, Soo KC, Chow PKH, Panasci L, Tran E. Xenografts of human hepatocellular carcinoma: a useful model for testing drugs. Clin Cancer Res 2006;12:4306-4314.

6) Wei W, Wu S, Wang X, Sun CK-W, Yang X, Yan X, et al. Novel celastrol derivatives inhibit the growth of hepatocellular carcinoma patient-derived xenografts. Oncotarget 2014;5:5819-5831.

7) **Gu Q, Zhang B,** Sun H, Xu Q, Tan Y, Wang G, et al. Genomic characterization of a large panel of patient-derived hepatocellular carcinoma xenograft tumor models for preclinical development. Oncotarget 2015;6:20160-20176.

8) Yan M, Li H, Zhao F, Zhang L, Ge C, Yao M, et al. Establishment of NOD/SCID mouse models of human hepatocellular carcinoma via subcutaneous transplantation of histologically intact tumor tissue. Chin J Cancer Res 2013;25:289-298.

9) Yang JD, Kim WR, Coelho R, Mettler TA, Benson JT, Sanderson SO, et al. Cirrhosis is present in most patients with hepatitis B and hepatocellular carcinoma. Clin Gastroenterol Hepatol 2011;9:64-70.

10) **Sonoshita M, Scopton AP,** Ung PMU, Murray MA, Silber L, Maldonado AY, et al. A whole-animal platform to advance a clinical kinase inhibitor into new disease space. Nat Chem Biol 2018;14:291-298.

11) Huynh H, Ong R, Zopf D. Antitumor activity of the multikinase inhibitor regorafenib in patient-derived xenograft models of gastric cancer. J Exp Clin Cancer Res 2015;34:132.

12) Li H, Durbin R. Fast and accurate short read alignment with Burrows-Wheeler transform. Bioinformatics 2009;25:1754-1760.

13) DePristo MA, Banks E, Poplin R, Garimella KV, Maguire JR, Hartl C, et al. A framework for variation discovery and genotyping using next-generation DNA sequencing data. Nat Genet 2011;43:491-498.

14) McKenna A, Hanna M, Banks E, Sivachenko A, Cibulskis K, Kernytsky A, et al. The Genome Analysis Toolkit: a MapReduce framework for analyzing next-generation DNA sequencing data. Genome Res 2010;20:1297-1303.

15) Van der Auwera GA, Carneiro MO, Hartl C, Poplin R, Del Angel G, Levy-Moonshine A, et al. From FastQ data to high confidence variant calls: the Genome Analysis Toolkit best practices pipeline. Curr Protoc Bioinformatics 2013;11:11.10.1-11.10.33.

16) Cibulskis K, Lawrence MS, Carter SL, Sivachenko A, Jaffe D, Sougnez C, et al. Sensitive detection of somatic point mutations in impure and heterogeneous cancer samples. Nat Biotechnol 2013;31:213-219.

17) Koboldt DC, Zhang Q, Larson DE, Shen D, McLellan MD, Lin L, et al. VarScan 2: somatic mutation and copy number alteration discovery in cancer by exome sequencing. Genome Res 2012;22:568-576.

18) Hansen NF, Gartner JJ, Mei L, Samuels Y, Mullikin JC. Shimmer: detection of genetic alterations in tumors using next-generation sequence data. Bioinformatics 2013;29:1498-1503.

19) Chiang C, Layer RM, Faust GG, Lindberg MR, Rose DB, Garrison EP, et al. SpeedSeq: ultra-fast personal genome analysis and interpretation. Nat Methods 2015;12:966-968.

20) Chen X, Schulz-Trieglaff O, Shaw R, Barnes B, Schlesinger F, Källberg M, et al. Manta: rapid detection of structural variants and indels for germline and cancer sequencing applications. Bioinformatics 2016;32:1220-1222.

21) Saunders CT, Wong WSW, Swamy S, Becq J, Murray LJ, Cheetham RK. Strelka: accurate somatic small-variant calling from sequenced tumor-normal sample pairs. Bioinformatics 2012;28:1811-1817.

22) Wang K, Li M, Hakonarson H. ANNOVAR: functional annotation of genetic variants from high-throughput sequencing data. Nucleic Acids Res 2010;38:e164.

23) Kim D, Langmead B, Salzberg SL. HISAT: a fast spliced aligner with low memory requirements. Nat Methods 2015;12:357-360.

24) Dobin A, Davis CA, Schlesinger F, Drenkow J, Zaleski C, Jha S, et al. STAR: ultrafast universal RNA-seq aligner. Bioinformatics 2013;29:15-21.

25) Harrow J, Frankish A, Gonzalez JM, Tapanari E, Diekhans M, Kokocinski F, et al. GENCODE: the reference human genome annotation for The ENCODE Project. Genome Res 2012;22:1760-1774.

26) Liao Y, Smyth GK, Shi W. featureCounts: an efficient general purpose program for assigning sequence reads to genomic features. Bioinformatics 2014;30:923-930.

27) McCarthy DJ, Chen Y, Smyth GK. Differential expression analysis of multifactor RNA-Seq experiments with respect to biological variation. Nucleic Acids Res 2012;40:4288-4297.

28) **Robinson MD**, **McCarthy DJ**, Smyth GK. edgeR: a Bioconductor package for differential expression analysis of digital gene expression data. Bioinformatics 2010;26:139-140.

29) **Subramanian A**, **Tamayo P**, Mootha VK, Mukherjee S, Ebert BL, Gillette MA, et al. Gene set enrichment analysis: a knowledge-based approach for interpreting genome-wide expression profiles. Proc Natl Acad Sci U S A 2005;102:15545-15550.

30) An C, Choi YA, Choi D, Paik YH, Ahn SH, Kim M-J, et al. Growth rate of early-stage hepatocellular carcinoma in patients with chronic liver disease. Clin Mol Hepatol 2015;21:279-286.

31) Azuma H, Paulk N, Ranade A, Dorrell C, Al-Dhalimy M, Ellis E, et al. Robust expansion of human hepatocytes in Fah–/–/Rag2–/–/Il2rg–/– mice. Nat Biotechnol 2007;25:903-910.

32) Grompe M, Lindstedt S, al-Dhalimy M, Kennaway NG, Papaconstantinou J, Torres-Ramos CA, et al. Pharmacological correction of neonatal lethal hepatic dysfunction in a murine model of hereditary tyrosinaemia type I. Nat Genet 1995;10:453-460.

33) Trojan J, Waidmann O. Role of regorafenib as second-line therapy and landscape of investigational treatment options in advanced hepatocellular carcinoma. J Hepatocell Carcinoma 2016;3:31-36.

Author names in bold designate shared co-first authorship.

Supporting Information

Additional Supporting Information may be found at onlinelibrary.wiley.com/doi/10.1002/hep.31096/suppinfo.